Acta Crystallographica Section D
Biological Crystallography
ISSN 1399-0047

X-ray structures of eIF5B and the eIF5B–eIF1A complex: the conformational flexibility of eIF5B is restricted on the ribosome by interaction with eIF1A

Aiping Zheng,[a]‡ Jian Yu,[a,b] Reo Yamamoto,[a] Toyoyuki Ose,[a,b] Isao Tanaka[a,b] and Min Yao[a,b]*

[a]Graduate School of Life Sciences, Hokkaido University, Kita 10 Nishi 8 Kita-Ku, Sapporo, Hokkaido 060-0810, Japan, and [b]Faculty of Advanced Life Sciences, Hokkaido University, Kita 10 Nishi 8 Kita-Ku, Sapporo, Hokkaido 060-0810, Japan

‡ Present address: McArdle Laboratory, Department of Oncology, School of Medicine and Public Health, University of Wisconsin at Madison, Madison, WI 53706, USA.

Correspondence e-mail: yao@castor.sci.hokudai.ac.jp

Received 13 March 2014
Accepted 29 September 2014

PDB references: eIF5B, 3wbi; 3wbj; eIF5B–eIF1A, 3wbk

eIF5B and eIF1A are two translation-initiation factors that are universally conserved among all kingdoms. They show a unique interaction in eukaryotes which is important for ribosomal subunit joining. Here, the structures of two isolated forms of yeast eIF5B and of the eIF5B–eIF1A complex (eIF1A and eIF5B do not contain the respective N-terminal domains) are reported. The eIF5B–eIF1A structure shows that the C-terminal tail of eIF1A binds to eIF5B domain IV, while the core domain of eIF1A is invisible in the electron-density map. Although the individual domains in all structures of eIF5B or archaeal IF5B (aIF5B) are similar, their domain arrangements are significantly different, indicating high structural flexibility, which is advantageous for conformational change during ribosomal subunit joining. Based on these structures, models of eIF5B, eIF1A and $tRNA_i^{Met}$ on the 80S ribosome were built. The models suggest that the interaction between the eIF1A C-terminal tail and eIF5B helps $tRNA_i^{Met}$ to bind to eIF5B domain IV, thus preventing $tRNA_i^{Met}$ dissociation, stabilizing the interface for subunit joining and providing a checkpoint for correct ribosome assembly.

1. Introduction

The initiation of protein synthesis on the ribosome is an important process for all living cells, and can be divided into two substages: start-codon selection and ribosomal subunit joining. This process requires at least 12 initiation factors in eukaryotes (eIFs), only two of which, eIF5B and eIF1A, are universally conserved among all three kingdoms (Jackson *et al.*, 2010).

eIF5B is a ribosome-dependent GTPase which was first identified in *Saccharomyces cerevisiae* (Choi *et al.*, 1998; Pestova *et al.*, 2000). Its bacterial and archaeal homologues are IF2 and aIF5B, respectively. *Escherichia coli* IF2 is essential for viability (Shiba *et al.*, 1986), while eIF5B is critically important but nonessential for cellular growth in *S. cerevisiae* (Choi *et al.*, 1998). eIF5B, as well as its archaeal homologue (aIF5B) and bacterial IF2, have been found to promote ribosomal subunit joining in the initiation process (Pestova *et al.*, 2000; Kolakofsky *et al.*, 1968). In addition, bacterial IF2 has another important function, *i.e.* recruitment (Lucas-Lenard, 1971) and stabilization (Simonetti *et al.*, 2008) of Met-$tRNA^{fMet}$ on the 30S subunit, while this function is accomplished by a dissimilar translation-initiation factor, eIF2 (consisting of α, β and γ subunits), in eukaryotes (Weissbach & Ochoa, 1976). Moreover, it has been reported that eIF5B can also promote Met-$tRNA_i^{Met}$ binding to the ribosome (Choi *et al.*, 1998).

During the initiation process in eukaryotes, after recognition of the start codon, eIF5B binds to the 48S pre-initiation complex (PIC), which is formed by the 40S ribosomal subunit, mRNA, initiator tRNA and several initiation factors. Subsequently, eIF5B promotes binding of the 60S ribosomal subunit, which triggers the hydrolysis of eIF5B-bound GTP, and eIF5B–GDP then leaves the ribosome, resulting in an 80S initiation complex (IC) ready for the next elongation stage (Pestova *et al.*, 2000).

Previous studies have shown that archaeal aIF5B consists of four domains and that domains I–III are connected to domain IV *via* a long helix, forming a 'chalice-shaped' structure (Roll-Mecak *et al.*, 2000). Domain I is the GTP-binding domain (G domain), while domain IV is necessary and sufficient for binding to initiator tRNA (Guillon *et al.*, 2005). Moreover, eIF5B and most nonthermophilic bacterial IF2s contain an additional divergent N-terminal region (N domain) that is thought to stabilize binding of IF2/eIF5B to the ribosome (Moreno *et al.*, 1999; Caserta *et al.*, 2006; Laalami *et al.*, 1991; Lee *et al.*, 1999) and is necessary for stable ribosomal subunit joining (Simonetti, Marzi, Billas *et al.*, 2013). Although the full-length crystal structure of IF2 is still not available, the core part of the structure of IF2 in apo, GDP-bound and GTP-bound states (Simonetti, Marzi, Fabbretti *et al.*, 2013) and the structure of the core part plus domain III of IF2 in apo and GDP-bound states (Eiler *et al.*, 2013) have been determined. The cryo-EM structure of a bacterial 70S–IF2 complex showed that IF2 is located at the inter-subunit cleft of the 70S ribosome (Allen *et al.*, 2005; Myasnikov *et al.*, 2005). The G domain of IF2 binds to the GTPase-associated centre (GAC centre) of the 50S subunit in a manner similar to elongation factors EF-G and EF-Tu, domain II binds to the 30S subunit, domain III is sandwiched between the subunits and domain IV interacts with the CCA end of the initiator tRNA. The conformation of IF2 (Allen *et al.*, 2005; Myasnikov *et al.*, 2005; Simonetti, Marzi, Billas *et al.*, 2013) and eIF5B (Fernández *et al.*, 2013) on the ribosome is very different from the crystal structure of IF2 and aIF5B, and also from the SAXS model of full-length IF2 off the ribosome (Simonetti, Marzi, Billas *et al.*, 2013).

eIF1A is a member of the oligonucleotide/oligosaccharide-binding fold (OB-fold) family of RNA-associated proteins (Battiste *et al.*, 2000; Hoffman & Li, 2001). The activities of eIF1A and its bacterial homologue IF1 are known to be essential for cellular life (Cummings & Hershey, 1994; Wei *et al.*, 1995). eIF1A plays multiple roles throughout the initiation process; it stimulates the binding of the (Met-tRNA$_i^{Met}$)–eIF2–GTP ternary complex to the 40S subunit (Olsen *et al.*, 2003), promotes scanning and start-codon selection together with eIF1 (Pestova *et al.*, 1998; Passmore *et al.*, 2007) and stimulates ribosome subunit joining (Acker *et al.*, 2006). It has been reported that IF1, eIF1A and their archaeal homologue aIF1A share a common OB-fold domain formed by a five-stranded β-barrel (Sette *et al.*, 1997; Battiste *et al.*, 2000; Hoffman & Li, 2001). External to the β-barrel, aIF1A additionally contains a helical subdomain at its C-terminus and an unstructured N-terminal tail (NTT) (Hoffman & Li, 2001). Furthermore, eIF1A contains an extra C-terminal tail (CTT) compared with aIF1A (Battiste *et al.*, 2000). The positively charged NTT and the negatively charged CTT of eIF1A have opposing effects on the stringency of start-codon selection. On the 40S ribosomal subunit, eIF1A binds to the top of rRNA helix 44, which is similar to the position of IF1 on the 30S subunit (Carter *et al.*, 2001; Weisser *et al.*, 2013). A direct contact is established between the helical subdomain of eIF1A and the head region of the 40S subunit, creating a bridge over the mRNA channel, which is distinguished from bacterial IF1 on the 30S subunit. Conserved residues in the NTT of eIF1A interact with two ribosomal proteins that have no bacterial homologues, and the CTT of eIF1A after residue 116 is invisible and probably only become structured after binding to the interaction partner in 43S PIC (Weisser *et al.*, 2013).

In bacteria, IF1 and IF2 can be cross-linked on the ribosome (Boileau *et al.*, 1983), and the binding affinity of IF2 for the 30S subunit is enhanced by the presence of IF1 (Sperling-Petersen *et al.*, 1999; Caserta *et al.*, 2006). Recently reported cryo-EM structures of 30S and 70S IC suggested a contact between IF1 and domain III of IF2 on the 30S subunit (Simonetti, Marzi, Billas *et al.*, 2013); however, no interaction between IF1 and IF2 was reported in solution. In contrast, eIF5B and eIF1A interact with each other directly even off the ribosome, and the interaction is mainly through their C-terminal domains (Choi *et al.*, 2000; Olsen *et al.*, 2003; Marintchev *et al.*, 2003). This interaction is required for efficient ribosomal subunit joining both *in vitro* and *in vivo* (Acker *et al.*, 2006; Fringer *et al.*, 2007). It has been proposed that this interaction is critical for accurate and efficient translation initiation by directing or stabilizing the binding of initiator tRNA to the ribosomal P-site (Choi *et al.*, 2000; Shin *et al.*, 2002). Moreover, mutation of either isoleucine residue of the last five residues DIDDI in the eIF1A C-terminus reduces GTP hydrolysis of eIF5B during the initiation process and affects subunit joining activity, whereas changing the aspartic acid residues has no effect (Acker *et al.*, 2006).

To understand the details of the interaction between eIF5B and eIF1A and how the interaction facilitates ribosomal subunit joining, we determined the structures of isolated eIF5B and the eIF5B–eIF1A complex from *S. cerevisiae*. The structure of eIF5B–eIF1A shows that the C-terminal tail of eIF1A binds to eIF5B domain IV. These structures reveal the high structural flexibility of eIF5B off the ribosome, especially domain IV. Finally, we built a binding model of eIF5B, eIF1A and initiator tRNA on the 80S ribosome based on the present structures and ribosome structures. We also discuss the advantages of eIF5B flexibility and the function of the interaction between the C-termini of eIF5B and eIF1A.

2. Methods

2.1. Protein preparation and crystallization

Expression and purification of eIF5B and eIF1A, preparation of the eIF5B–eIF1A complex and crystallization of eIF5B and the eIF5B–eIF1A complex were performed as described previously (Zheng *et al.*, 2011). The eIF5B-2 crystals were

grown at 293 K by sitting-drop vapour diffusion against 0.1 *M* Tris–HCl pH 8.2, 40% PEG 400, 0.2 *M* Li_2SO_4 with the eIF5B–eIF1A complex at a concentration of 42 mg ml^{-1}. The crystals belonged to space group $P6_122$ and contained one molecule per asymmetric unit with 51% solvent content.

2.2. Data collection, structure determination and refinement

Preliminary X-ray analyses of eIF5B-1 and the eIF5B–eIF1A complex were performed as described previously (Zheng *et al.*, 2011), where eIF5B-1 is called eIF5BΔN, and were reprocessed using *XDS* (Kabsch, 2010). X-ray diffraction data for the eIF5B-2 crystals were collected on beamline BL41XU at SPring-8, Japan under cryoconditions (Proposal Nos. 2010A1046 and 2011A1299). The diffraction data were indexed, integrated, scaled and merged using *XDS*.

The structure of eIF5B-1 was solved by the Se-SAD method (Zheng *et al.*, 2011). Phasing of eIF5B-2 and the eIF5B–eIF1A complex was carried out by the molecular-replacement method with *MOLREP* (Vagin & Teplyakov, 2010) in the *CCP*4 program suite. As the structure of eIF5B is highly flexible, we failed to determine the structures of eIF5B-2 and the eIF5B–eIF1A complex using the whole structure of eIF5B-1 as the search model. The structure of eIF5B-1 was divided into three parts: domains I–II, domain III and domain IV. Firstly, domain I–II was used as a search model and the solution was found. Domain III was then used as a further search model with domain I–II as a fixed molecule in the target crystal structure. Finally, domain IV of eIF5B-1 was used as the search model with domains I–II and III as fixed molecules. The solution of domain IV was found in eIF5B–eIF1A but not in eIF5B-2. Further model building, fitting and refinement were then carried out automatically using the program *LAFIRE* (Yao *et al.*, 2006) running with the refinement program *CNS* (Brunger, 2007). In particular, for the eIF5B–eIF1A complex, after refining eIF5B in several cycles, a distinct peptide-like electron-density blob was found in both $2F_o - F_c$ and $F_o - F_c$ maps close to helices 13 and 14 of eIF5B (molecule *A*) domain IV, which is thought to be the eIF1A binding region. Therefore, we built the C-terminal tail of eIF1A (residues Gly143–Ile153) into the map blob by several cycles of manual model checking and fitting with the graphics program *Coot* (Emsley *et al.*, 2010). Moreover, the refinement of the eIF5B–eIF1A complex was performed under different conditions such as with and without the restraint of maximum *B*-factor limitation, omitting and rebuilding the C-terminal tail of eIF1A and parts of eIF5B, and using *REFMAC*5 (Murshudov *et al.*, 2011), *phenix_refine* (Afonine *et al.*, 2012) and *autoBUSTER* (Bricogne *et al.*, 2011). The results showed that *REFMAC*5 provided the best result, with a lower R_{free} factor and a clear electron-density map for the C-terminal tail of eIF1A without the restraint of maximum *B*-factor limitation, even if the averaged *B* factor is high. Final TLS refinement (Winn *et al.*, 2001) for each molecule in an asymmetric unit was performed in the last several cycles with *REFMAC*5 for eIF5B-1 and for the eIF5B–eIF1A complex and with *phenix_refine* for eIF5B-2.

2.3. Binding model of ribosome with eIF5B and eIF1A

To build the model of eIF5B and eIF1A complexed with the ribosome in the GTP-bound state, domains I–IV of eIF5B molecule *A* were superposed onto the corresponding parts of eIF5B in the cryo-EM structure of the eukaryotic translation-initiation complex (Fernández *et al.*, 2013; PDB entries 4byt, 4byx, 4byu, 4byv and 4byw), which also has a P/I-state initiator tRNA bound to it. Helix 8 of eIF5B, which connects domain II and domain III, was partially turned into a loop in the C-terminus. eIF1A from the 40S–eIF1–eIF1A complex (Weisser *et al.*, 2013; PDB entry 4bpe) was then added to the model by 18S superposition. The eIF1A C-terminal tail, which was partially visible in the binding site of the current eIF5B–eIF1A complex structure, was also added.

2.4. PDB depositions

Atomic coordinates and structure factors have been deposited in the Protein Data Bank as the following entries: eIF5B-1, 3wbi; eIF5B-2, 3wbj; eIF5B–eIF1A complex, 3wbk.

3. Results

3.1. Overall structure of eIF5B

As the flexible region in eIF5B and eIF1A may hamper the production of high-quality crystals, we expressed N-terminal domain-truncated eIF5B (residues 401–1002) and N-terminal tail-truncated eIF1A (residues 27–153). For simplicity, the N-terminally truncated eIF5B and eIF1A are referred to as 'eIF5B' and 'eIF1A' throughout this report. X-ray-quality crystals were grown from isolated eIF5B and its complex with eIF1A (Zheng *et al.*, 2011). Two crystal forms of isolated eIF5B, referred to as eIF5B-1 and eIF5B-2, were obtained. They both have one molecule in the asymmetric unit. The structure of eIF5B-1 was determined by Se-SAD phasing (Zheng *et al.*, 2011), while that of eIF5B-2 was determined by molecular replacement. The structure of eIF5B-1 in the apo form (GTP/GDP-free form) is shown in Fig. 1(*a*). It was refined at 2.35 Å resolution to a free *R* factor of 26.8% and an *R* factor of 21.0% using native data (Table 1). The final refined structure consists of residues 401–477 and 492–1002 and 98 water molecules. Residues 78–91 could not be built owing to a poor electron-density map. The overall structure of eIF5B-1 has dimensions of 92 × 68 × 42 Å and consists of four different domains (domains I, II, III and IV). Domain I (residues 401–625), which is the GTP-binding domain (G domain), has a P-loop and two switch regions, which are common motifs of G proteins.

It is well known that the switch 1 region of G proteins is responsible for interaction with effectors. In the case of eIF5B, the effector is the ribosome. The electron-density map clearly showed that the conformation of the switch 1 region (Gly432–Gly443) of eIF5B-1 is different from that of aIF5B, which is partially invisible even in the GTP-bound state (Roll-Mecak *et al.*, 2000). The map of residues Pro478–Ser491 within the switch 2 region of eIF5B-1 (Asp476–Cys494) was not shown clearly in the $2F_o - F_c$ and $F_o - F_c$ maps owing to the

flexibility of switch 2 without GTP binding. Previous results also showed that switch 2 of aIF5B is partially invisible in the apo form and has a poor electron-density map in the GDP-bound form, but is stable in the GTP-bound form, with a lower average *B* factor than that of the entire G domain (Roll-Mecak *et al.*, 2000).

Domain II (residues 630–724) of eIF5B-1 is an EF-Tu domain II-like β-barrel barrel and is connected to domain III *via* helix 8 (H8), which has a kink in the middle. Domain III (residues 753–834) is an α–β–α sandwich structure connected through the 32 Å long helix H12 to domain IV (residues 864–1002), which is an antiparallel β-barrel with nine strands followed by two α-helices (Fig. 1*b*). Domains I, II and III of eIF5B-1 individually show structural similarity to those of aIF5B, with root-mean-square deviations (r.m.s.d.s) on C^{α} atoms of 0.976, 0.708 and 0.814, respectively, while domain IV shows greater structural differences, with an r.m.s.d. of 1.828. Compared with aIF5B, β23, β24 and the loop between β27 and β28 are longer in eIF5B-1, and the C-terminal helices H13 and H14 are parallel to each other. In the eIF5B-1 structure, the long helix H12, which connects domains III and IV, is shorter than that in aIF5B, and the six C-terminal residues of H12 form a flexible loop. The position of domain II relative to domain I deviates slightly from that in aIF5B, whereas the position of domain III relative to domain II is rotated by ∼38° around a hinge region (hinge 1) between H9 and switch 2 compared with the aIF5B structure (Figs. 2*a* and 2*b*).

Unlike the 'chalice-shaped' structure of aIF5B (Roll-Mecak *et al.*, 2000), domain IV of eIF5B-1 rotates around the flexible loop (hinge 2, residues 856–861) which connects domain IV and α12, and is packed against domain III (Supplementary

Table 1
Statistics of data collection, phasing and refinement.

Values in parentheses are for the last resolution shell.

	eIF5B-1	eIF5B-2	eIF5B–eIF1A
Data collection			
Wavelength (Å)	1.000	0.979	
Space group	$P4_12_12$	$P6_122$	
Unit-cell parameters (Å)	$a = b = 129.6$, $c = 70.5$	$a = b = 120.7$, $c = 168.2$	
Resolution (Å)	43.2–2.35 (2.49–2.35)	44.4–2.49 (2.65–2.49)	
Completeness (%)	99.6 (97.6)	99.6 (98.0)	
Unique reflections	25590	25847	
$\langle I/\sigma(I)\rangle$	22.4 (3.2)	35.1 (7.3)	
Multiplicity	14.1 (14.3)	23.3 (23.0)	
R_{merge}† (%)	9.1 (99.7)	8.0 (52.0)	
Refinement			
Resolution range (Å)	41.0–2.35	44.4–2.50	40.0–3.30
R_{work} (%)	21.0	20.2	26.1
R_{free}‡ (%)	26.8	24.7	31.7
R.m.s.d. from ideal geometry			
Bond lengths (Å)	0.008	0.005	0.008
Bond angles (°)	1.113	0.938	1.306
Ramachandran plot (%)			
Preferred	96.58	97.00	96.43
Allowed	3.25	3.00	3.57
Outliers	0.17	0.00	0.00

† $R_{merge} = \sum_{hkl}\sum_i |I_i(hkl) - \langle I(hkl)\rangle| / \sum_{hkl}\sum_i I_i(hkl)$, where $\langle I(hkl)\rangle$ is the mean intensity of a set of equivalent reflections. ‡ R_{free} was calculated using a test data set consisting of a randomly selected 7% of the total reflections that were excluded from refinement.

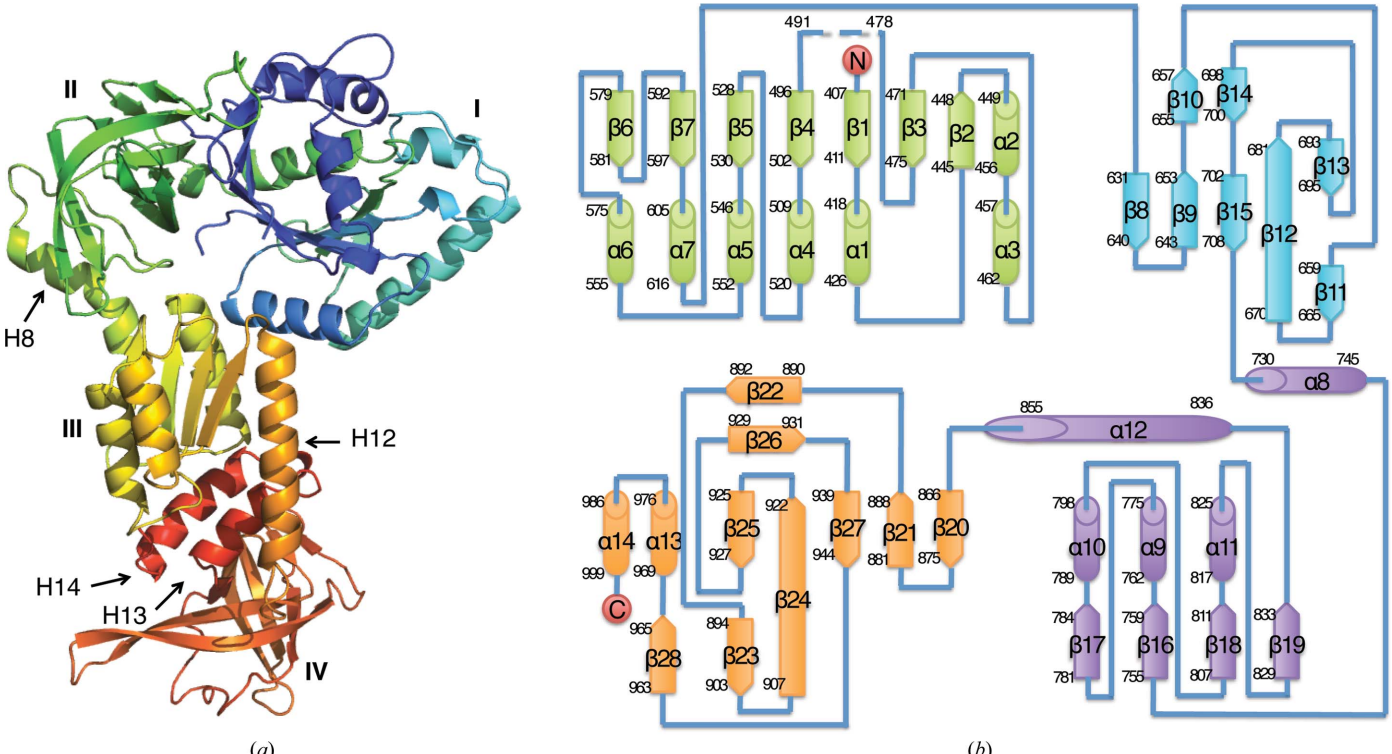

Figure 1
Structure and topology of eIF5B-1. (*a*) Structure of the N-terminal domain-truncated eIF5B-1 from *S. cerevisiae* in the apo form. The C^{α} trace is rainbow-coloured from the N-terminus (blue) to the C-terminus (red). Helices 8, 12, 13 and 14 are indicated by arrows. (*b*) Secondary structure of eIF5B-1. Domains I, II, III and IV are shown in green, cyan, purple and orange, respectively.

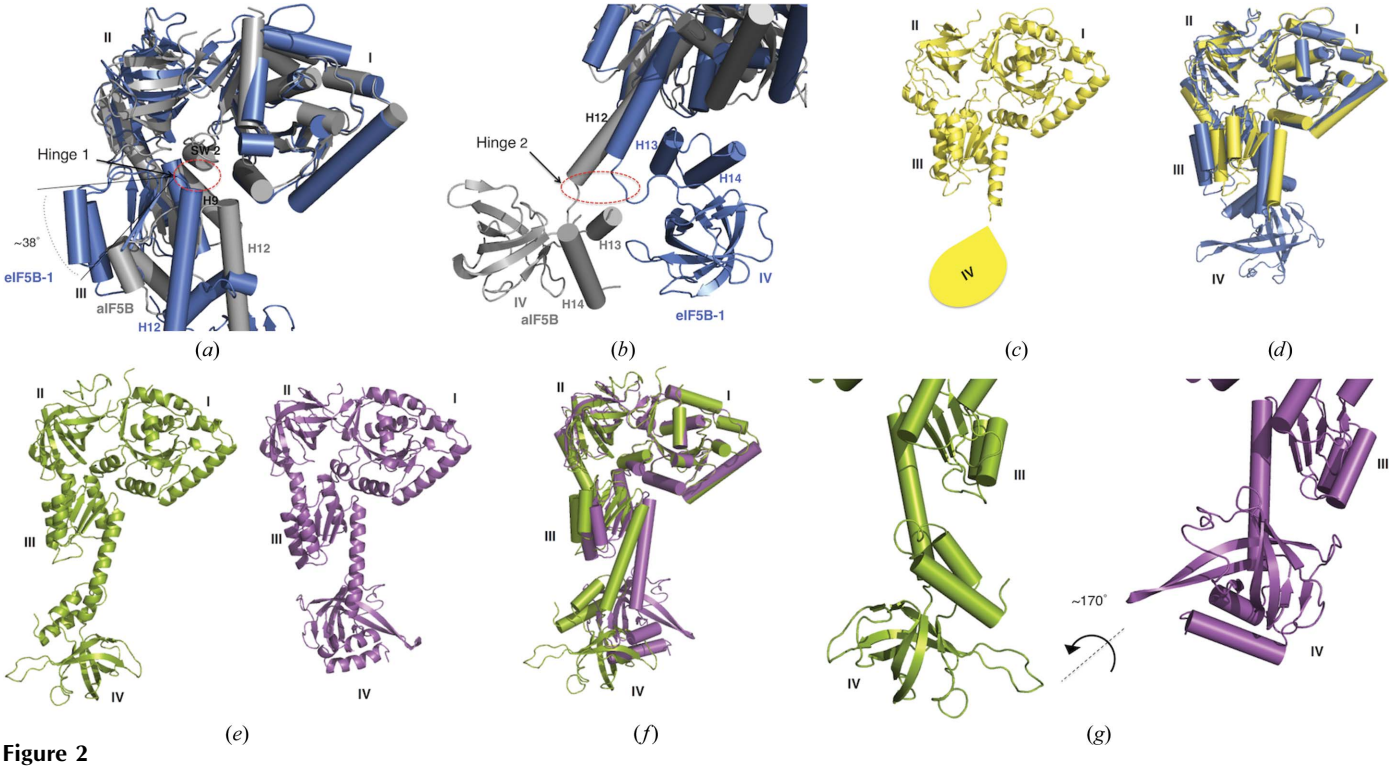

Figure 2
Conformational flexibility of eIF5B. (*a*) Rotation of domain III around the hinge 1 region shown by superposition of eIF5B-1 (blue) and aIF5B–GDPNP (grey) domain I. (*b*) Rotation of domain IV around the hinge 2 region shown by superposition of eIF5B-1 (blue) and aIF5B–GDPNP (grey; PDB entry 1g7t) domain III. (*c*) Structure of the N-terminal domain-truncated eIF5B-2 from *S. cerevisiae* in the apo form. Domain IV of eIF5B-2 could not be built, suggesting that it is highly flexible. (*d*) Superposition of eIF5B-2 (yellow) and eIF5B (blue) by the G domain shows movement of domain III around the hinge 1 region. (*e*) Structures of two eIF5B molecules in the asymmetric unit of the eIF5B–eIF1A complex crystal. The two eIF5B molecules are referred to as molecule *A* (left) and molecule *B* (right). (*f*) Superposition of molecule *A* and molecule *B* by domain I. Molecule *A* and molecule *B* are shown in green and magenta, respectively. (*g*) Conformational differences of domain IV between molecule *A* (left) and molecule *B* (right). Domain I of molecule *A* and molecule *B* are superposed (domains I–II are not shown.)

Fig. S1). Two C-terminal helices (H13 and H14) of domain IV, which is thought to bind to the C-terminal tail of eIF1A (Marintchev *et al.*, 2003), are close to the surface of domain III and consequently the binding site is buried inside the molecule (Fig. 1*a*).

The structure of eIF5B-2 in the apo form is shown in Fig. 2(*c*). It was refined at 2.49 Å resolution to a free *R* factor of 24.7% and an *R* factor of 20.2% (Table 1). The final refined structure of eIF5B-2 consists of residues 401–478, 482–684 and 692–855 and 125 water molecules; domain IV (residues 856–1002), however, is invisible. To exclude the possibility that domain IV was proteolytically degraded during crystallization, TOF-MS of redissolved crystals of eIF5B-2 was performed (Supplementary Fig. S2). The results verified the presence of domain IV in the crystal (Zheng *et al.*, 2011). Moreover, residues 479–481 and 685–691 also could not be built owing to a poor electron-density map. Although the domains of eIF5B-2 are structurally similar to the corresponding domains of eIF5B-1 (r.m.s.d.s on C^{α} atoms of 0.686 Å for domain I, 0.453 Å for domain II and 0.945 Å for domain III), the whole conformation is different. Domain III of eIF5B-2 is rotated by ∼20° relative to domain I–II around the hinge 1 region compared with eIF5B-1 (Fig. 2*d*).

[1] Supporting information has been deposited in the IUCr electronic archive (Reference: MH5136).

Domain IV of eIF5B-2 (residues 856–1002), which is connected to helix 12 through the hinge 2 region, could not be built, suggesting that it is very flexible and can adopt multiple conformations. Owing to crystal packing, the nucleotide-binding sites of two nearby eIF5B-2 molecules in the crystal are close to each other, resulting a space that is is only large enough for one guanine nucleotide, although the binding sites are not blocked. The conformation of switch 1 of eIF5B-2, which is thought to be flexible, is similar to that of eIF5B-1 (Supplementary Fig. S3), although the packing in the two crystals is different.

3.2. Interaction between eIF5B and eIF1A

The crystals of the eIF5B–eIF1A complex grew in the presence of PEG 3350, and the crystal content was confirmed by SDS–PAGE (Zheng *et al.*, 2011). There are two eIF5B molecules in the asymmetric unit, referred to as molecule *A* and molecule *B*, respectively (Fig. 2*e*). While the position of the eIF1A core was difficult to locate owing to a poor electron-density map, the C-terminal tail of eIF1A, which binds to domain IV of molecule *A*, could be built based on both $2F_o - F_c$ and $F_o - F_c$ maps. In order to avoid misbuilding, model rebuilding was carried out repeatedly using OMIT maps calculated by different refinement programs. All OMIT maps showed the presence of the C-terminal tail of eIF1A

(Supplementary Fig. S4), although the refined *B* factors of the eIF1A C-terminal tail were high. Finally, the structure of the eIF5B–eIF1A complex was refined at 3.30 Å resolution to a free *R* factor of 31.7% and an *R* factor of 26.1% (Table 1). The present refined model consists of residues 402–429 and 435–1002 of molecule *A*, residues 402–428, 437–685 and 689–1002 of molecule *B* and residues 143–153 of eIF1A. One region of molecule *A* (residues 430–434) and two regions of molecule *B* (residues 429–436 and 686–688), as well as residues 27–142 of eIF1A, could not be built owing to a poor electron-density map.

Similar to the structures of eIF5B-1 and eIF5B-2, the individual domains of molecule *A* and molecule *B* were also similar, but the overall conformations of molecule *A* and molecule *B* were different. Fig. 2(*f*) shows a superposition of the G domain between molecule *A* and molecule *B*. The rotation of domain II is relatively small, while the rotations of domain III and domain IV are significant. Domain III rotates ∼13° around the hinge 1 region, while domain IV is rotated ∼170° relative to domain III around the hinge 2 region and faces in almost the opposite direction (Fig. 2*g*). Unlike eIF5B-1 and eIF5B-2, part of the switch 1 region of molecule *A* (residues 430–434) and molecule *B* (residues 429–436) shows poor electron density, indicating that this region is flexible. The conformations of the switch 2 regions of molecule *A* and molecule *B* are different, suggesting that the conformation of switch 2 is variable in the nucleotide-free structures.

Moreover, in the present eIF5B–eIF1A complex structure the C-terminal tail was only bound to molecule *A* in the asymmetric unit. In domain IV of molecule *B*, the binding pocket of the eIF1A C-terminal tail was turned to the opposite side to that in molecule *A* and the C-terminal tail of eIF1A was not observed. As shown in Fig. 3 and Supplementary Fig. S5, the C-terminal tail (11 residues) of eIF1A binds to a pocket (eIF1A tail binding pocket) formed by two helices (H13 and H14) in domain IV of eIF5B (molecule *A*). The abundance of hydrophobic residues in the binding site indicates that the interaction between eIF5B domain IV and the eIF1A C-terminus is mainly hydrophobic (Fig. 3*b*). Leu148, Ile150 and Ile153 of eIF1A interact with Ile972, Phe980, Trp989 and Leu990 of eIF5B. Among these hydrophobic residues, the importance of Ile150 and Ile153 of eIF1A and Ile972 and Trp989 of eIF5B have been confirmed by previous research using NMR (Marintchev *et al.*, 2003) and biochemical experiments (Acker *et al.*, 2006). In addition to the hydrophobic interaction, hydrogen bonds are also found between the eIF5B side chains and the eIF1A main chain. The side chains of the conserved residues Arg969 and Lys976 of eIF5B are positioned within hydrogen-bonding distance of the main chains of Ile150 and Ile153 in eIF1A. Therefore, the residues Ile150 and Ile153 within the eIF1A C-terminal peptide DIDDI are involved in both hydrophobic and hydrophilic interactions with eIF5B.

3.3. Models of the 80S–eIF5B–eIF1A complex

The binding model was built based on superposition of known structures and biochemical data. In the GTP-bound model (Fig. 4), both the eIF1A C-terminal tail and the initiator tRNA acceptor arm bind to the eIF5B domain IV, forming a

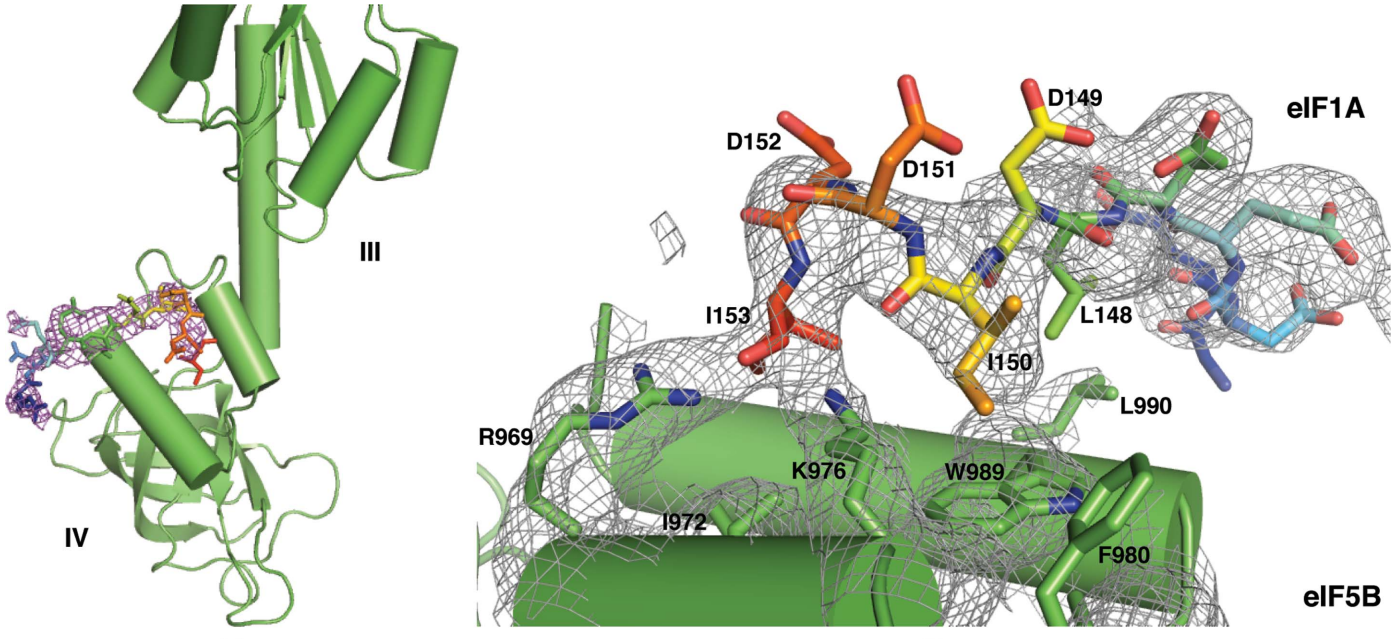

(*a*) (*b*)

Figure 3
Interaction between eIF5B and eIF1A. (*a*) The C-terminus of eIF1A binds to eIF5B molecule *A* domain IV in the eIF5B–eIF1A complex crystal. eIF5B molecule *A* is shown in green. The C-terminus of eIF1A is shown as sticks rainbow-coloured from the N-terminus (blue) to the C-terminus (red). The $F_o - F_c$ map around residues 143–153 of eIF1A is shown in magenta at a contour of 2.0σ. (*b*) Close-up of the eIF5B and eIF1A binding site with a feature-enhanced map at contour of 1.0σ (http://www.phenix-online.org/presentations/fem.pdf).

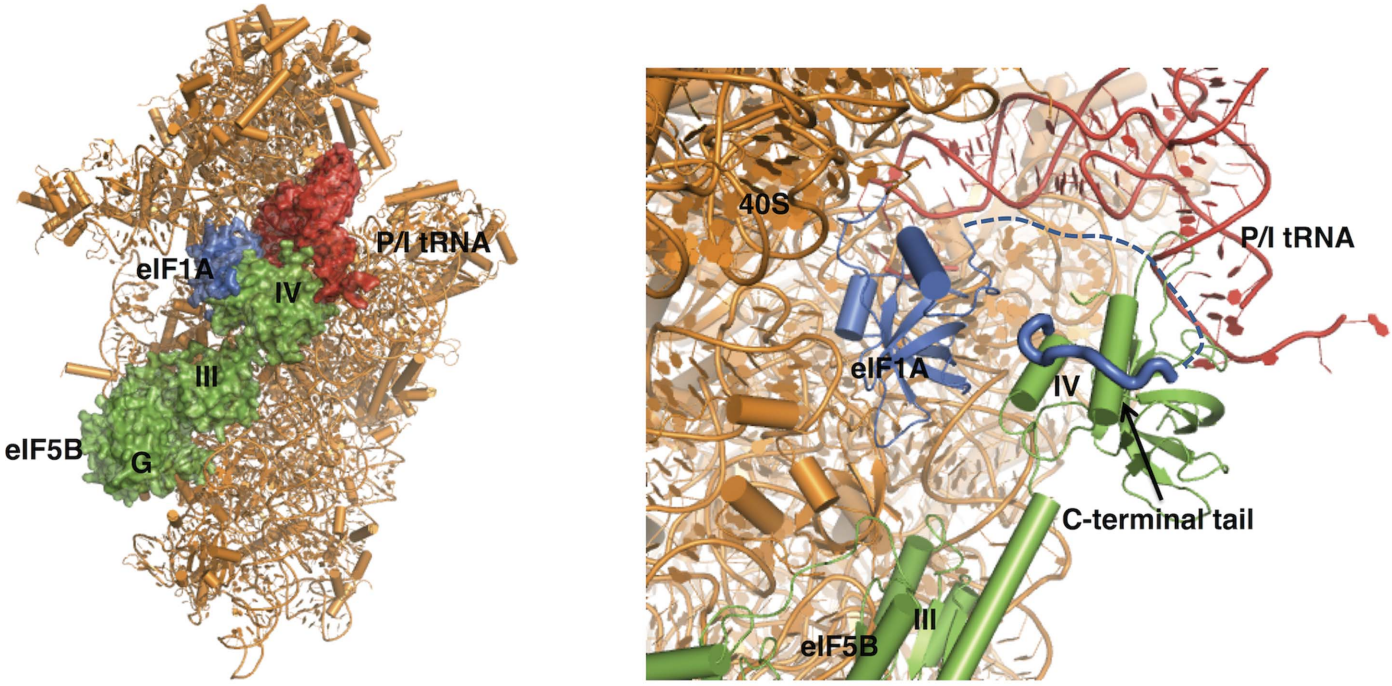

Figure 4
eIF5B binding model on the 80S ribosome. (*a*) eIF5B–eIF1A–initiator–tRNA binding model on the 80S ribosome in the GTP-bound state. (*b*) Close-up of the binding site. Both the eIF1A C-terminal tail and the initiator tRNA acceptor arm bind to eIF5B domain IV, forming a stable tripod. The 60S subunit was removed for clarity. eIF5B is shown in green, P/I-state tRNA in red, eIF1A in blue and the 40S subunit in orange. The part of eIF1A C-terminal tail that connects the eIF1A core region to the last 11 residues of eIF1A that bind to eIF5B domain IV is shown as a dashed line.

stable tripod ready for guiding ribosome subunit joining in a rotated conformation as in IF2 (Marshall *et al.*, 2009).

4. Discussion

4.1. Conformational flexibility of eIF5B

A superposition of all five structures of eIF5B and its homologue, aIF5B, by G-domain arrangement is shown in Supplementary Fig. S6. Although the individual domains of the five structures are similar, their overall conformations are different. In particular, domain III and domain IV rotate around two hinge regions in all structures. The moderate rotation of domain III causes the long helix H12 to point in different directions, while domain IV, which is more flexible, rotates in different directions (domain IV of eIF5B-2 is invisible) in all structures, suggesting that the conformation of domain IV in solution is dynamic. On the other hand, the positions of domain II relative to domain I among the eIF5B structures are similar, although there is a small rotation compared with aIF5B. Such conformational relationships may reflect the conformational change requirement of eIF5B between the pre- and post-state of ribosomal subunit joining, as reported for IF2 on the 30S ribosome subunit before and after 50S subunit joining (Simonetti *et al.*, 2008).

The recently solved structure of the core region and domain III of IF2 in two conformations also shows large-scale conformational changes off the ribosome (Eiler *et al.*, 2013). Domain IV of IF2 is invisible in the crystal structure, similar to that of eIF5B-2, indicating that domain IV of IF2 is also flexible off the ribosome. In addition, the variation of domain III locations in different IF2 conformations is more apparent than that of eIF5B, possibly because helix 8 of IF2, which connects domain II and III, is much longer than that in eIF5B. The 'articulated lever' mechanism proposed previously for aIF5B suggested that the 'chalice-shaped' aIF5B functions as a molecular lever and amplifies the modest conformational change in domain G caused by GTP hydrolysis to domain IV through a long distance (Eiler *et al.*, 2013). However, the high flexibility of eIF5B and IF2 domains III and IV off the ribosome reported here and several recently published papers have challenged this mechanism, since domain III and domain IV adopt a different orientation in solution regardless of the presence or absence of binding of GTP/GDP. This indicates that the 'articulated lever' mechanism may only exist in archaea, or that the structure of aIF5B may also be flexible and the previous solved crystal structure of aIF5B only represents one of its conformations in solution.

Besides eIF5B and its archaeal homologue aIF5B, the selenocysteine tRNA-specific elongation factor SelB also has the special 'chalice-shaped' structure (Leibundgut *et al.*, 2005). Interestingly, SelB also shows some conformational flexibility off the ribosome. The orientation of domain IV in two different SelB molecules in the asymmetric unit varies by a rotation of about 20°. Therefore, the high degree of flexibility may be a substantial property of molecules with a 'chalice-shaped' structure. Such flexibility may be useful for the formation of a 'molecular bridge' with its partner: with the

initiator tRNA in the case of eIF5B and with the SECIS (selenocysteine-inserting sequence) element in the case of SelB.

4.2. Models of eIF5B and eIF1A bound to the ribosome

All of the conformations of isolated eIF5B and aIF5B solved by crystallization are different from that of the cryo-EM structure of the translation-initiation complex (Fernández *et al.*, 2013). Isolated eIF5B is highly flexible and dynamic, and transforms between different conformations in solution so that several possible conformations of isolated eIF5B were captured during crystallization. When eIF5B binds to the ribosome, domains G and II are fixed and domain III moves to a different position. This domain rearrangement requires the disorder of the C-terminal half of helix 8 (residues Asp740–Ser747), which is semi-conserved among eukaryotes. Disorder of the C-terminus of helix 8 was observed in the extended conformation of IF2 (Eiler *et al.*, 2013), and it causes a distinct orientation of domain III compared with that in the compact conformation. However, as shown in the multiple structures of eIF5B and IF2, the conformation of helix 8 in eIF5B is not as flexible as that in IF2, so this conformational change in eIF5B possibly only occurs during binding to the ribosome. Domain IV of eIF5B is still dynamic, even with the binding of the eIF1A C-terminal tail. eIF5B domain IV binds to initiation tRNA and adopts a stable conformation that was observed in the cryo-EM structure of the translation-initiation complex (Fernández *et al.*, 2013).

Based on structural superposition of the ribosome in complex with translation factors and the biochemical data, we built a model representing the GTP-bound state of eIF5B bound to the 80S ribosome, which is composed of the 80S ribosome, eIF5B, eIF1A and initiator tRNA (Fig. 4). In the GTP-state model, the eIF1A C-terminal tail and the acceptor arm of initiator tRNA bind simultaneously to domain IV of eIF5B and form a stable tripod, thus stabilizing and/or orienting the initiator tRNA to adopt a hybrid P/I state ready for guiding ribosome subunit joining in a rotated conformation as in IF2 (Marshall *et al.*, 2009).

It was proposed that the joining of the 60S subunit induces hydrolysis of eIF5B-bound GTP, which may cause rotation of eIF5B domain II and domain III *via* a conformational change of switch 2, while movement of domain III is transmitted to domain IV *via* the long helix and causes domain IV to dissociate from the initiator tRNA. Then, the initiator tRNA back-translocates into the P/P state ready for formation of the first peptide bond and the ribosome is driven back into the nonrotated conformation. The conformational change of the 80S complex also loosens the binding of eIF1A and promotes the rapid release of eIF1A (Acker *et al.*, 2009), whereas eIF5B dissociates from the ribosome coupled with eIF1A.

4.3. Function of the interaction between eIF5B and the eIF1A C-terminal tail

The eIF1A C-terminal tail interacts with eIF5B domain IV and restricts the high flexibility of eIF5B domain IV during the last assembly stage. Meanwhile, the length of the eIF1A C-terminal tail (∼40 residues) may make the eIF5B domain IV free to move above the surface of the ribosome and thus result in conformational changes of eIF5B on the ribosome, which are required for 60S subunit joining, and also the subsequent hydrolysis of GTP-bound eIF5B. This type of structure, a long tail with the binding region at its end, has also been reported in other ribosome-related proteins such as the ribosomal stalk complex P0/P1 (Nomura *et al.*, 2012).

Interaction between eIF5B and eIF1A in the crystal was observed between eIF5B domain IV and the eIF1A C-terminal tail. However, it is difficult to locate the eIF1A core domain, suggesting that the core domain may make no stable interactions with eIF5B. In the model of eIF5B and eIF1A interaction on the ribosome built in the present study, the core domain of eIF1A also makes no direct interactions with eIF5B, indicating that the interaction between the C-termini of the proteins may be the only interaction important for their functions on the ribosome.

The interaction between eIF5B and the C-terminal tail of eIF1A is unique to eukaryotes. Obviously, this interaction promotes binding of eIF5B to the 40S subunit in eukaryotes (Fringer *et al.*, 2007). However, it is not clear why it is not necessary in bacteria or archaea, and the biological significance of the evolution of this new interaction between two universally conserved initiation factors remains unclear.

In eukaryotes, eIF5B domain IV is considered to bind to initiator tRNA on the ribosomal small subunit, similar to its bacterial homologue IF2. However, the binding affinity between them is very low (K_d = 40 μM) compared with those of their bacterial and archaeal homologues, which are in the micromolar range (Guillon *et al.*, 2005; Krafft *et al.*, 2000). In addition, the highly flexible properties of eIF5B domain IV may make its binding to initiator tRNA more difficult. Thus, the interaction between eIF1A and eIF5B domain IV in eukaryotes may be involved in stabilizing binding between eIF5B and initiator tRNA (Fig. 4). The stabilized binding between eIF5B domain IV and initiator tRNA could prevent the dissociation of initiator tRNA before ribosomal subunit joining and provide a stable interface for 60S subunit binding. It may also be a checkpoint for the correct assembly of the 80S initiation complex.

We thank Dr Massaki Sokabe for preparing the vectors of eIF5B and eIF1A. AZ was supported by the International Graduate Program for Research Pioneers in Life Sciences (IGP-RPLS) and this project was supported by a Grant-in-Aid for Scientific Research (B) (25291008 to MY) from the Ministry of Education, Culture, Sports, Science and Technology of Japan.

References

Acker, M. G., Shin, B.-S., Dever, T. E. & Lorsch, J. R. (2006). *J. Biol. Chem.* **281**, 8469–8475.

Acker, M. G., Shin, B.-S., Nanda, J. S., Saini, A. K., Dever, T. E. & Lorsch, J. R. (2009). *J. Mol. Biol.* **385**, 491–506.

Afonine, P. V., Grosse-Kunstleve, R. W., Echols, N., Headd, J. J., Moriarty, N. W., Mustyakimov, M., Terwilliger, T. C., Urzhumtsev, A., Zwart, P. H. & Adams, P. D. (2012). *Acta Cryst.* D**68**, 352–367.

Allen, G. S., Zavialov, A., Gursky, R., Ehrenberg, M. & Frank, J. (2005). *Cell*, **121**, 703–712.

Battiste, J. L., Pestova, T. V., Hellen, C. U. T. & Wagner, G. (2000). *Mol. Cell*, **5**, 109–119.

Boileau, G., Butler, P., Hershey, J. W. & Traut, R. R. (1983). *Biochemistry*, **22**, 3162–3170.

Bricogne, G., Blanc, E., Brandl, M., Flensburg, C., Keller, P., Paciorek, W., Roversi, P., Sharff, A., Smart, O. S., Vonrhein, C. & Womack, T. O. (2011). *AutoBUSTER*. Cambridge: Global Phasing Ltd.

Brunger, A. T. (2007). *Nature Protoc.* **2**, 2728–2733.

Carter, A. P., Clemons, W. M., Brodersen, D. E., Morgan-Warren, R. J., Hartsch, T., Wimberly, B. T. & Ramakrishnan, V. (2001). *Science*, **291**, 498–501.

Caserta, E., Tomsic, J., Spurio, R., La Teana, A., Pon, C. L. & Gualerzi, C. O. (2006). *J. Mol. Biol.* **362**, 787–799.

Choi, S. K., Lee, J. H., Zoll, W. L., Merrick, W. C. & Dever, T. E. (1998). *Science*, **280**, 1757–1760.

Choi, S. K., Olsen, D. S., Roll-Mecak, A., Martung, A., Remo, K. L., Burley, S. K., Hinnebusch, A. G. & Dever, T. E. (2000). *Mol. Cell. Biol.* **20**, 7183–7191.

Cummings, H. S. & Hershey, J. W. B. (1994). *J. Bacteriol.* **176**, 198–205.

Eiler, D., Lin, J., Simonetti, A., Klaholz, B. P. & Steitz, T. A. (2013). *Proc. Natl Acad. Sci. USA*, **110**, 15662–15667.

Emsley, P., Lohkamp, B., Scott, W. G. & Cowtan, K. (2010). *Acta Cryst.* D**66**, 486–501.

Fernández, I. S., Bai, X.-C., Hussain, T., Kelley, A. C., Lorsch, J. R., Ramakrishnan, V. & Scheres, S. H. W. (2013). *Science*, **342**, 1240585.

Fringer, J. M., Acker, M. G., Fekete, C. A., Lorsch, J. R. & Dever, T. E. (2007). *Mol. Cell. Biol.* **27**, 2384–2397.

Guillon, L., Schmitt, E., Blanquet, S. & Mechulam, Y. (2005). *Biochemistry*, **44**, 15594–15601.

Hoffman, D. W. & Li, W. (2001). *Protein Sci.* **10**, 2426–2438.

Jackson, R. J., Hellen, C. U. T. & Pestova, T. V. (2010). *Nature Rev. Mol. Cell Biol.* **11**, 113–127.

Kabsch, W. (2010). *Acta Cryst.* D**66**, 125–132.

Kolakofsky, D., Ohta, T. & Thach, R. E. (1968). *Nature (London)*, **220**, 244–247.

Krafft, C., Diehl, A., Laettig, S., Behlke, J., Heinemann, U., Pon, C. L., Gualerzi, C. O. & Welfle, H. (2000). *FEBS Lett.* **471**, 128–132.

Laalami, S., Sacerdot, C., Vachon, G., Mortensen, K., Sperling-Petersen, H. U., Cenatiempo, Y. & Grunberg-Manago, M. (1991). *Biochimie*, **73**, 1557–1566.

Lee, J. H., Choi, S. K., Roll-Mecak, A., Burley, S. K. & Dever, T. E. (1999). *Proc. Natl Acad. Sci. USA*, **96**, 4342–4347.

Leibundgut, M., Frick, C., Thanbichler, M., Böck, A. & Ban, N. (2005). *EMBO J.* **24**, 11–22.

Lucas-Lenard, J. (1971). *Annu. Rev. Biochem.* **40**, 409–448.

Marintchev, A., Kolupaeva, V. G., Pestova, T. V. & Wagner, G. (2003). *Proc. Natl Acad. Sci. USA*, **100**, 1535–1540.

Marshall, R. A., Aitken, C. E. & Puglisi, J. D. (2009). *Mol. Cell*, **35**, 37–47.

Moreno, J. M., Drskjøtersen, L., Kristensen, J. E., Mortensen, K. K. & Sperling-Petersen, H. U. (1999). *FEBS Lett.* **455**, 130–134.

Murshudov, G. N., Skubák, P., Lebedev, A. A., Pannu, N. S., Steiner, R. A., Nicholls, R. A., Winn, M. D., Long, F. & Vagin, A. A. (2011). *Acta Cryst.* D**67**, 355–367.

Myasnikov, A. G., Marzi, S., Simonetti, A., Giuliodori, A. M., Gualerzi, C. O., Yusupova, G., Yusupov, M. & Klaholz, B. P. (2005). *Nature Struct. Mol. Biol.* **12**, 1145–1149.

Nomura, N., Honda, T., Baba, K., Naganuma, T., Tanzawa, T., Arisaka, F., Noda, M., Uchiyama, S., Tanaka, I., Yao, M. & Uchiumi, T. (2012). *Proc. Natl Acad. Sci. USA*, **109**, 3748–3753.

Olsen, D. S., Savner, E. M., Mathew, A., Zhang, F., Krishnamoorthy, T., Phan, L. & Hinnebusch, A. G. (2003). *EMBO J.* **22**, 193–204.

Passmore, L. A., Schmeing, T. M., Maag, D., Applefield, D. J., Acker, M. G., Algire, M. A., Lorsch, J. R. & Ramakrishnan, V. (2007). *Mol. Cell*, **26**, 41–50.

Pestova, T. V., Borukhov, S. I. & Hellen, C. U. T. (1998). *Nature (London)*, **394**, 854–859.

Pestova, T. V., Lomakin, I. B., Lee, J. H., Choi, S. K., Dever, T. E. & Hellen, C. U. T. (2000). *Nature (London)*, **403**, 332–335.

Roll-Mecak, A., Cao, C., Dever, T. E. & Burley, S. K. (2000). *Cell*, **103**, 781–792.

Sette, M., van Tilborg, P., Spurio, R., Kaptein, R., Paci, M., Gualerzi, C. O. & Boelens, R. (1997). *EMBO J.* **16**, 1436–1443.

Shiba, K., Ito, K., Nakamura, Y., Dondon, J. & Grunberg-Manago, M. (1986). *EMBO J.* **5**, 3001–3006.

Shin, B. S., Maag, D., Roll-Mecak, A., Arefin, M. S., Burley, S. K., Lorsch, J. R. & Dever, T. E. (2002). *Cell*, **111**, 1015–1025.

Simonetti, A., Marzi, S., Billas, I. M., Tsai, A., Fabbretti, A., Myasnikov, A. G., Roblin, P., Vaiana, A. C., Hazemann, I., Eiler, D., Steitz, T. A., Puglisi, J. D., Gualerzi, C. O. & Klaholz, B. P. (2013). *Proc. Natl Acad. Sci. USA*, **110**, 15656–15661.

Simonetti, A., Marzi, S., Fabbretti, A., Hazemann, I., Jenner, L., Urzhumtsev, A., Gualerzi, C. O. & Klaholz, B. P. (2013). *Acta Cryst.* D**69**, 925–933.

Simonetti, A., Marzi, S., Myasnikov, A. G., Fabbretti, A., Yusupov, M., Gualerzi, C. O. & Klaholz, B. P. (2008). *Nature (London)*, **455**, 416–420.

Sperling-Petersen, H. U., Moreno, J. M. P., Dyrskjotersen, L., Kristensen, J. E. & Mortensen, K. K. (1999). *FEBS Lett.* **455**, 130–134.

Vagin, A. & Teplyakov, A. (2010). *Acta Cryst.* D**66**, 22–25.

Wei, C.-L., Kainuma, M. & Hershey, J. W. (1995). *J. Biol. Chem.* **270**, 22788–22794.

Weissbach, H. & Ochoa, S. (1976). *Annu. Rev. Biochem.* **45**, 191–216.

Weisser, M., Voigts-Hoffmann, F., Rabl, J., Leibundgut, M. & Ban, N. (2013). *Nature Struct. Mol. Biol.* **20**, 1015–1017.

Winn, M. D., Isupov, M. N. & Murshudov, G. N. (2001). *Acta Cryst.* D**57**, 122–133.

Yao, M., Zhou, Y. & Tanaka, I. (2006). *Acta Cryst.* D**62**, 189–196.

Zheng, A., Yamamoto, R., Sokabe, M., Tanaka, I. & Yao, M. (2011). *Acta Cryst.* F**67**, 730–733.